Amplitude analysis of the $\chi_{c1} \to \eta\pi^+\pi^-$ decays

M. Ablikim[1], M. N. Achasov[9,e], S. Ahmed[14], X. C. Ai[1], O. Albayrak[5], M. Albrecht[4], D. J. Ambrose[44], A. Amoroso[49A,49C], F. F. An[1], Q. An[46,a], J. Z. Bai[1], O. Bakina[23], R. Baldini Ferroli[20A], Y. Ban[31], D. W. Bennett[19], J. V. Bennett[5], N. Berger[22], M. Bertani[20A], D. Bettoni[21A], J. M. Bian[43], F. Bianchi[49A,49C], E. Boger[23,c], I. Boyko[23], R. A. Briere[5], H. Cai[51], X. Cai[1,a], O. Cakir[40A], A. Calcaterra[20A], G. F. Cao[1], S. A. Cetin[40B], J. Chai[49C], J. F. Chang[1,a], G. Chelkov[23,c,d], G. Chen[1], H. S. Chen[1], J. C. Chen[1], M. L. Chen[1,a], S. Chen[41], S. J. Chen[29], X. Chen[1,a], X. R. Chen[26], Y. B. Chen[1,a], H. P. Cheng[17], X. K. Chu[31], G. Cibinetto[21A], H. L. Dai[1,a], J. P. Dai[34], A. Dbeyssi[14], D. Dedovich[23], Z. Y. Deng[1], A. Denig[22], I. Denysenko[23], M. Destefanis[49A,49C], F. De Mori[49A,49C], Y. Ding[27], C. Dong[30], J. Dong[1,a], L. Y. Dong[1], M. Y. Dong[1,a], Z. L. Dou[29], S. X. Du[53], P. F. Duan[1], J. Z. Fan[39], J. Fang[1,a], S. S. Fang[1], X. Fang[46,a], Y. Fang[1], R. Farinelli[21A,21B], L. Fava[49B,49C], F. Feldbauer[22], G. Felici[20A], C. Q. Feng[46,a], E. Fioravanti[21A], M. Fritsch[14,22], C. D. Fu[1], Q. Gao[1], X. L. Gao[46,a], Y. Gao[39], Z. Gao[46,a], I. Garzia[21A], K. Goetzen[10], L. Gong[30], W. X. Gong[1,a], W. Gradl[22], M. Greco[49A,49C], M. H. Gu[1,a], Y. T. Gu[12], Y. H. Guan[1], A. Q. Guo[1], L. B. Guo[28], R. P. Guo[1], Y. Guo[1], Y. P. Guo[22], Z. Haddadi[25], A. Hafner[22], S. Han[51], X. Q. Hao[15], F. A. Harris[42], K. L. He[1], F. H. Heinsius[4], T. Held[4], Y. K. Heng[1,a], T. Holtmann[4], Z. L. Hou[1], C. Hu[28], H. M. Hu[1], J. F. Hu[49A,49C], T. Hu[1,a], Y. Hu[1], G. S. Huang[46,a], J. S. Huang[15], X. T. Huang[33], X. Z. Huang[29], Y. Huang[29], Z. L. Huang[27], T. Hussain[48], W. Ikegami Andersson[50], Q. Ji[1], Q. P. Ji[15], X. B. Ji[1], X. L. Ji[1,a], L. W. Jiang[51], X. S. Jiang[1,a], X. Y. Jiang[30], J. B. Jiao[33], Z. Jiao[17], D. P. Jin[1,a], S. Jin[1], T. Johansson[50], A. Julin[43], N. Kalantar-Nayestanaki[25], X. L. Kang[1], X. S. Kang[30], M. Kavatsyuk[25], B. C. Ke[5], P. Kiese[22], R. Kliemt[10], B. Kloss[22], O. B. Kolcu[40B,h], B. Kopf[4], M. Kornicer[42], A. Kupsc[50], W. Kühn[24], J. S. Lange[24], M. Lara[19], P. Larin[14], H. Leithoff[22], C. Leng[49C], C. Li[50], Cheng Li[46,a], D. M. Li[53], F. Li[1,a], F. Y. Li[31], G. Li[1], H. B. Li[1], H. J. Li[1], J. C. Li[1], Jin Li[32], K. Li[33], K. Li[13], Lei Li[3], P. R. Li[41], Q. Y. Li[33], T. Li[33], W. D. Li[1], W. G. Li[1], X. L. Li[33], X. N. Li[1,a], X. Q. Li[30], Y. B. Li[2], Z. B. Li[38], H. Liang[46,a], Y. F. Liang[36], Y. T. Liang[24], G. R. Liao[11], D. X. Lin[14], B. Liu[34], B. J. Liu[1], C. X. Liu[1], D. Liu[46,a], F. H. Liu[35], Fang Liu[1], Feng Liu[6], H. B. Liu[12], H. H. Liu[1], H. H. Liu[16], H. M. Liu[1], J. Liu[1], J. B. Liu[46,a], J. P. Liu[51], J. Y. Liu[1], K. Liu[39], K. Y. Liu[27], L. D. Liu[31], P. L. Liu[1,a], Q. Liu[41], S. B. Liu[46,a], X. Liu[26], Y. B. Liu[30], Y. Y. Liu[30], Z. A. Liu[1,a], Zhiqing Liu[22], H. Loehner[25], Y. F. Long[31], X. C. Lou[1,a,g], H. J. Lu[17], J. G. Lu[1,a], Y. Lu[1], Y. P. Lu[1,a], C. L. Luo[28], M. X. Luo[52], T. Luo[42], X. L. Luo[1,a], X. R. Lyu[41], F. C. Ma[27], H. L. Ma[1], L. L. Ma[33], M. M. Ma[1], Q. M. Ma[1], T. Ma[1], X. N. Ma[30], X. Y. Ma[1,a], Y. M. Ma[33], F. E. Maas[14], M. Maggiora[49A,49C], Q. A. Malik[48], Y. J. Mao[31], Z. P. Mao[1], S. Marcello[49A,49C], J. G. Messchendorp[25], G. Mezzadri[21B], J. Min[1,a], T. J. Min[1], R. E. Mitchell[19], X. H. Mo[1,a], Y. J. Mo[6], C. Morales Morales[14], N. Yu. Muchnoi[9,e], H. Muramatsu[43], P. Musiol[4], Y. Nefedov[23], F. Nerling[10], I. B. Nikolaev[9,e], Z. Ning[1,a], S. Nisar[8], S. L. Niu[1,a], X. Y. Niu[1], S. L. Olsen[32], Q. Ouyang[1,a], S. Pacetti[20B], Y. Pan[46,a], P. Patteri[20A], M. Pelizaeus[4], H. P. Peng[46,a], K. Peters[10,i], J. Pettersson[50], J. L. Ping[28], R. G. Ping[1], R. Poling[43], V. Prasad[1], H. R. Qi[2], M. Qi[29], S. Qian[1,a], C. F. Qiao[41], L. Q. Qin[33], N. Qin[51], X. S. Qin[1], Z. H. Qin[1,a], J. F. Qiu[1], K. H. Rashid[48], C. F. Redmer[22], M. Ripka[22], G. Rong[1], Ch. Rosner[14], X. D. Ruan[12], A. Sarantsev[23,f], M. Savrié[21B], C. Schnier[4], K. Schoenning[50], S. Schumann[22], W. Shan[31], M. Shao[46,a], C. P. Shen[2], P. X. Shen[30], X. Y. Shen[1], H. Y. Sheng[1], M. Shi[1], W. M. Song[1], X. Y. Song[1], S. Sosio[49A,49C], S. Spataro[49A,49C], G. X. Sun[1], J. F. Sun[15], S. S. Sun[1], X. H. Sun[1], Y. J. Sun[46,a], Y. Z. Sun[1], Z. J. Sun[1,a], Z. T. Sun[19], C. J. Tang[36], X. Tang[1], I. Tapan[40C], E. H. Thorndike[44], M. Tiemens[25], I. Uman[40D], G. S. Varner[42], B. Wang[30], B. L. Wang[41], D. Wang[31], D. Y. Wang[31], K. Wang[1,a], L. L. Wang[1], L. S. Wang[1], M. Wang[33], P. Wang[1], P. L. Wang[1], W. Wang[1,a], W. P. Wang[46,a], X. F. Wang[39], Y. Wang[37], Y. D. Wang[14], Y. F. Wang[1,a], Y. Q. Wang[22], Z. Wang[1,a], Z. G. Wang[1,a], Z. H. Wang[46,a], Z. Y. Wang[1], Z. Y. Wang[1], T. Weber[22], D. H. Wei[11], P. Weidenkaff[22], S. P. Wen[1], U. Wiedner[4], M. Wolke[50], L. H. Wu[1], L. J. Wu[1], Z. Wu[1,a], L. Xia[46,a], L. G. Xia[39], Y. Xia[18], D. Xiao[1], H. Xiao[47], Z. J. Xiao[28], Y. G. Xie[1,a], Q. L. Xiu[1,a], G. F. Xu[1], J. J. Xu[1], L. Xu[1], Q. J. Xu[13], Q. N. Xu[41], X. P. Xu[37], L. Yan[49A,49C], W. B. Yan[46,a], W. C. Yan[46,a], Y. H. Yan[18], H. J. Yang[34,j], H. X. Yang[1], L. Yang[51], Y. X. Yang[11], M. Ye[1,a], M. H. Ye[7], J. H. Yin[1], Z. Y. You[38], B. X. Yu[1,a], C. X. Yu[30], J. S. Yu[26], C. Z. Yuan[1], W. L. Yuan[29], Y. Yuan[1], A. Yuncu[40B,b], A. A. Zafar[48], A. Zallo[20A], Y. Zeng[18], Z. Zeng[46,a], B. X. Zhang[1], B. Y. Zhang[1,a], C. Zhang[29], C. C. Zhang[1], D. H. Zhang[1], H. H. Zhang[38], H. Y. Zhang[1,a], J. Zhang[1], J. J. Zhang[1], J. L. Zhang[1], J. Q. Zhang[1], J. W. Zhang[1,a], J. Y. Zhang[1], J. Z. Zhang[1], K. Zhang[1], L. Zhang[1], S. Q. Zhang[30], X. Y. Zhang[33], Y. Zhang[1], Y. Zhang[1], Y. H. Zhang[1,a], Y. N. Zhang[41], Y. T. Zhang[46,a], Yu Zhang[41], Z. H. Zhang[6], Z. P. Zhang[46], Z. Y. Zhang[51], G. Zhao[1], J. W. Zhao[1,a], J. Y. Zhao[1], J. Z. Zhao[1,a], Lei Zhao[46,a], Ling Zhao[1], M. G. Zhao[30], Q. Zhao[1], Q. W. Zhao[1], S. J. Zhao[53], T. C. Zhao[1], Y. B. Zhao[1,a], Z. G. Zhao[46,a], A. Zhemchugov[23,c], B. Zheng[47], J. P. Zheng[1,a], W. J. Zheng[33], Y. H. Zheng[41], B. Zhong[28], L. Zhou[1,a], X. Zhou[51], X. K. Zhou[46,a], X. R. Zhou[46,a], X. Y. Zhou[1], K. Zhu[1], K. J. Zhu[1,a], S. Zhu[1], S. H. Zhu[45],

arXiv:1610.02479v2 [hep-ex] 11 Oct 2016

X. L. Zhu[39], Y. C. Zhu[46,a], Y. S. Zhu[1], Z. A. Zhu[1], J. Zhuang[1,a], L. Zotti[49A,49C], B. S. Zou[1], J. H. Zou[1]

(BESIII Collaboration)

[1] *Institute of High Energy Physics, Beijing 100049, People's Republic of China*
[2] *Beihang University, Beijing 100191, People's Republic of China*
[3] *Beijing Institute of Petrochemical Technology, Beijing 102617, People's Republic of China*
[4] *Bochum Ruhr-University, D-44780 Bochum, Germany*
[5] *Carnegie Mellon University, Pittsburgh, Pennsylvania 15213, USA*
[6] *Central China Normal University, Wuhan 430079, People's Republic of China*
[7] *China Center of Advanced Science and Technology, Beijing 100190, People's Republic of China*
[8] *COMSATS Institute of Information Technology, Lahore, Defence Road, Off Raiwind Road, 54000 Lahore, Pakistan*
[9] *G.I. Budker Institute of Nuclear Physics SB RAS (BINP), Novosibirsk 630090, Russia*
[10] *GSI Helmholtzcentre for Heavy Ion Research GmbH, D-64291 Darmstadt, Germany*
[11] *Guangxi Normal University, Guilin 541004, People's Republic of China*
[12] *Guangxi University, Nanning 530004, People's Republic of China*
[13] *Hangzhou Normal University, Hangzhou 310036, People's Republic of China*
[14] *Helmholtz Institute Mainz, Johann-Joachim-Becher-Weg 45, D-55099 Mainz, Germany*
[15] *Henan Normal University, Xinxiang 453007, People's Republic of China*
[16] *Henan University of Science and Technology, Luoyang 471003, People's Republic of China*
[17] *Huangshan College, Huangshan 245000, People's Republic of China*
[18] *Hunan University, Changsha 410082, People's Republic of China*
[19] *Indiana University, Bloomington, Indiana 47405, USA*
[20] *(A)INFN Laboratori Nazionali di Frascati, I-00044, Frascati, Italy; (B)INFN and University of Perugia, I-06100, Perugia, Italy*
[21] *(A)INFN Sezione di Ferrara, I-44122, Ferrara, Italy; (B)University of Ferrara, I-44122, Ferrara, Italy*
[22] *Johannes Gutenberg University of Mainz, Johann-Joachim-Becher-Weg 45, D-55099 Mainz, Germany*
[23] *Joint Institute for Nuclear Research, 141980 Dubna, Moscow region, Russia*
[24] *Justus-Liebig-Universitaet Giessen, II. Physikalisches Institut, Heinrich-Buff-Ring 16, D-35392 Giessen, Germany*
[25] *KVI-CART, University of Groningen, NL-9747 AA Groningen, The Netherlands*
[26] *Lanzhou University, Lanzhou 730000, People's Republic of China*
[27] *Liaoning University, Shenyang 110036, People's Republic of China*
[28] *Nanjing Normal University, Nanjing 210023, People's Republic of China*
[29] *Nanjing University, Nanjing 210093, People's Republic of China*
[30] *Nankai University, Tianjin 300071, People's Republic of China*
[31] *Peking University, Beijing 100871, People's Republic of China*
[32] *Seoul National University, Seoul, 151-747 Korea*
[33] *Shandong University, Jinan 250100, People's Republic of China*
[34] *Shanghai Jiao Tong University, Shanghai 200240, People's Republic of China*
[35] *Shanxi University, Taiyuan 030006, People's Republic of China*
[36] *Sichuan University, Chengdu 610064, People's Republic of China*
[37] *Soochow University, Suzhou 215006, People's Republic of China*
[38] *Sun Yat-Sen University, Guangzhou 510275, People's Republic of China*
[39] *Tsinghua University, Beijing 100084, People's Republic of China*
[40] *(A)Ankara University, 06100 Tandogan, Ankara, Turkey; (B)Istanbul Bilgi University, 34060 Eyup, Istanbul, Turkey; (C)Uludag University, 16059 Bursa, Turkey; (D)Near East University, Nicosia, North Cyprus, Mersin 10, Turkey*
[41] *University of Chinese Academy of Sciences, Beijing 100049, People's Republic of China*
[42] *University of Hawaii, Honolulu, Hawaii 96822, USA*
[43] *University of Minnesota, Minneapolis, Minnesota 55455, USA*
[44] *University of Rochester, Rochester, New York 14627, USA*
[45] *University of Science and Technology Liaoning, Anshan 114051, People's Republic of China*
[46] *University of Science and Technology of China, Hefei 230026, People's Republic of China*
[47] *University of South China, Hengyang 421001, People's Republic of China*
[48] *University of the Punjab, Lahore-54590, Pakistan*

[49] (A)University of Turin, I-10125, Turin, Italy; (B)University of Eastern Piedmont, I-15121, Alessandria, Italy; (C)INFN, I-10125, Turin, Italy
[50] Uppsala University, Box 516, SE-75120 Uppsala, Sweden
[51] Wuhan University, Wuhan 430072, People's Republic of China
[52] Zhejiang University, Hangzhou 310027, People's Republic of China
[53] Zhengzhou University, Zhengzhou 450001, People's Republic of China

[a] Also at State Key Laboratory of Particle Detection and Electronics, Beijing 100049, Hefei 230026, People's Republic of China
[b] Also at Bogazici University, 34342 Istanbul, Turkey
[c] Also at the Moscow Institute of Physics and Technology, Moscow 141700, Russia
[d] Also at the Functional Electronics Laboratory, Tomsk State University, Tomsk, 634050, Russia
[e] Also at the Novosibirsk State University, Novosibirsk, 630090, Russia
[f] Also at the NRC "Kurchatov Institute", PNPI, 188300, Gatchina, Russia
[g] Also at University of Texas at Dallas, Richardson, Texas 75083, USA
[h] Also at Istanbul Arel University, 34295 Istanbul, Turkey
[i] Also at Goethe University Frankfurt, 60323 Frankfurt am Main, Germany
[j] Also at Institute of Nuclear and Particle Physics, Shanghai Key Laboratory for Particle Physics and Cosmology, Shanghai 200240, People's Republic of China

(Dated: October 12, 2016)

Using 448.0×10^6 $\psi(3686)$ events collected with the BESIII detector, an amplitude analysis is performed for $\psi(3686) \to \gamma\chi_{c1}$, $\chi_{c1} \to \eta\pi^+\pi^-$ decays. The most dominant two-body structure observed is $a_0(980)^\pm\pi^\mp$; $a_0(980)^\pm \to \eta\pi^\pm$. The $a_0(980)$ line shape is modeled using a dispersion relation, and a significant non-zero $a_0(980)$ coupling to the $\eta'\pi$ channel is measured. We observe $\chi_{c1} \to a_2(1700)\pi$ production for the first time, with a significance larger than 17σ. The production of mesons with exotic quantum numbers, $J^{PC} = 1^{-+}$, is investigated, and upper limits for the branching fractions $\chi_{c1} \to \pi_1(1400)^\pm\pi^\mp$, $\chi_{c1} \to \pi_1(1600)^\pm\pi^\mp$, and $\chi_{c1} \to \pi_1(2015)^\pm\pi^\mp$, with subsequent $\pi_1(X)^\pm \to \eta\pi^\pm$ decay, are determined.

PACS numbers: 13.25.Gv, 14.40.Be, 14.40.Pq, 14.40.Rt

I. INTRODUCTION

Charmonium decays provide a rich laboratory for light meson spectroscopy. Large samples of charmonium states with $J^{PC} = 1^{--}$, like the J/ψ and $\psi(3686)$, are easily produced at e^+e^- colliders, and their transitions provide sizable charmonium samples with other J^{PC} quantum numbers, like the χ_{c1} (1^{++}). The $\chi_{c1} \to \eta\pi\pi$ decay is suitable for studying the production of exotic mesons with $J^{PC} = 1^{-+}$, which could be observed decaying into the $\eta\pi$ final state. The lowest orbital excitation of a two-body combination in χ_{c1} decays to three pseudoscalars, for instance $\chi_{c1} \to \eta\pi\pi$, is the S-wave transition, in which if a resonance is produced, it has to have $J^{PC} = 1^{-+}$. Several candidates with $J^{PC} = 1^{-+}$, decaying into different final states, such as $\eta\pi$, $\eta'\pi$, $f_1(1270)\pi$, $b_1(1235)\pi$ and $\rho\pi$, have been reported by various experiments, and these have been thoroughly reviewed in Ref. [1]. The lightest exotic meson candidate is the $\pi_1(1400)$ [2], reported only in the $\eta\pi$ final state [3–5], but its resonance nature is controversial [6]. The most promising $J^{PC} = 1^{-+}$ candidate, the $\pi_1(1600)$ [2], could also couple to the $\eta\pi$, since it has been observed in the $\eta'\pi$ channel [7].

The CLEO-c Collaboration reported evidence of an exotic signal in $\chi_{c1} \to \eta'\pi^+\pi^-$ decays, consistent with $\pi_1(1600) \to \eta'\pi$ production [8]. However, other possible exotic signals that could be expected have not been observed in either $\chi_{c1} \to \eta\pi^+\pi^-$ or $\chi_{c1} \to \eta'\pi^+\pi^-$ decays. With a more than 15 times larger data sample at BESIII, there is an opportunity to search for the production of π_1 exotic mesons. In this work we investigate possible production of exotic mesons in the mass region (1.3-2.0) GeV/c^2, decaying into the $\eta\pi^+ + c.c.$ final state, namely the $\pi_1(1400)$, $\pi_1(1600)$, and $\pi_1(2015)$, using $\chi_{c1} \to \eta\pi^+\pi^-$ decays. Charge conjugation and isospin symmetry are assumed in this analysis.

Additional motivation for studying these decays is that a very prominent $a_0(980) \to \eta\pi$ signal of high purity was observed in $\chi_{c1} \to \eta\pi^+\pi^-$ [8]. The $a_0(980)$ was discovered several decades ago, but its nature is still not fully understood [9, 10]. The $a_0(980)$ decays dominantly into $\eta\pi$ and $K\bar{K}$ final states; the latter has a profound influence on the $a_0(980)$ line shape in the $\eta\pi$ channel, due to the proximity of the $K\bar{K}$ threshold to the $a_0(980)$ mass. Data from different experiments are analyzed [11, 12] to determine the couplings of the $a_0(980)$ to the $\eta\pi$ ($g_{\eta\pi}$) and $K\bar{K}$ final states ($g_{K\bar{K}}$), in order to help resolve the open question of whether the $a_0(980)$ is a four-quark state or $K\bar{K}$ molecule. However, the values

obtained for the $a_0(980)$ parameters vary considerably among various analyses [8, 11, 12]. Another channel of interest is $a_0(980) \to \eta'\pi$, with the threshold more than 100 MeV/c^2 above the $a_0(980)$ mass. The first direct observation of the decay $a_0(980) \to \eta'\pi$ was reported by CLEO-c [8], using a sample of 26×10^6 $\psi(3686)$ decays. The $a_0(980)$ coupling to the $\eta'\pi$ channel, $g_{\eta'\pi}$, was determined from $\chi_{c1} \to \eta\pi^+\pi^-$ decays, although the analysis was not very sensitive to the $a_0(980) \to \eta'\pi$ component in the $a_0(980) \to \eta\pi$ invariant mass distribution, and $g_{\eta'\pi}$ was found to be consistent with zero. In many analyses of $a_0(980)$ couplings, $g_{\eta'\pi}$ has not been measured. For example, its value was fixed in Ref. [12] based on SU(3) flavor-mixing predictions. Using a clean sample of χ_{c1} produced in the radiative transition $\psi(3686) \to \gamma\chi_{c1}$ at BESIII, we investigate the $\chi_{c1} \to \eta\pi^+\pi^-$ decays to test if the $a_0(980) \to \eta\pi$ invariant mass distribution is sensitive to $\eta'\pi$ production. Dispersion integrals in the description of the $a_0(980)$ line shape are used to determine the $a_0(980)$ parameters, its invariant mass, $m_{a_0(980)}$, and three coupling constants: $g_{\eta\pi}$, $g_{K\bar{K}}$ and $g_{\eta'\pi}$. This information might help in determining the quark structure of the $a_0(980)$.

In this χ_{c1} decay mode, it is also possible to study $\chi_{c1} \to a_2(1700)\pi$; $a_2(1700) \to \eta\pi$ production. The $a_2(1700)$ has been reported by different experiments in this decay mode [13], but still is not accepted as an established resonance by the Particle Data Group (PDG) [2].

II. EVENT SELECTION

For our studies we use $(448.0 \pm 3.1) \times 10^6$ $\psi(3686)$ events, collected in 2009 [14] and 2012 [15] with the BESIII detector [16]. We select 95% of possible η decays, in the $\eta \to \gamma\gamma$, $\eta \to \pi^+\pi^-\pi^0$ and $\eta \to \pi^0\pi^0\pi^0$ decay modes. For each $\psi(3686) \to \gamma\eta\pi^+\pi^-$ final state topology, exclusive Monte Carlo (MC) samples are generated according to the relative branching fractions given in Table I, equivalent to a total of 2×10^7 $\psi(3686) \to \gamma\chi_{c1}$; $\chi_{c1} \to \eta\pi^+\pi^-$ events. The background is studied using an inclusive MC sample of 106×10^6 generic $\psi(3686)$ events.

BESIII is a conventional solenoidal magnet detector that has almost full geometrical acceptance, and four main components: the main drift chamber (MDC), electromagnetic calorimeter (EMC), time-of-flight detector (TOF), all enclosed in 1 T magnetic field, and the muon chamber. The momentum resolution for 1 GeV/c charged particles is 0.5%, while the energy resolution for 1.0 GeV photons in the barrel (end-cap) region of the EMC is 2.5% (5%). Details of the BESIII detector and its performance can be found in Ref [16].

Good photon candidates are selected from isolated EMC showers with energy larger than 25 (50) MeV in the barrel (end-cap) region, corresponding to the polar angle, θ, satisfying $|\cos\theta| < 0.80$ ($0.86 < |\cos\theta| < 0.92$). The timing of good EMC showers is required to be within 700 ns of the trigger time. Charged tracks must satisfy $|\cos\theta| < 0.93$, and the point of closest approach of a track from the interaction point along the beam direction is required to be within 20 cm and within 2 cm perpendicular to the beam direction. All charged tracks are assumed to be pions, and the inclusive MC sample is used to verify that the kaon contamination in the final sample is negligible in each of the η channels. We require two charged tracks for the $\eta \to \gamma\gamma$ and $\eta \to 3\pi^0$ channels, and four tracks for the $\eta \to \pi^+\pi^-\pi^0$ channel, with zero net charge. For $\eta \to \gamma\gamma$ and $\eta \to \pi^+\pi^-\pi^0$, at least three photon candidates are required, and for $\eta \to 3\pi^0$ at least 7 photon candidates. The invariant mass of two-photon combinations is kinematically constrained to the π^0 or η mass.

The sum of momenta of all final-state particles, for a given final state topology, is constrained to the initial $\psi(3686)$ momentum. If multiple combinations for an event are found, the one with the smallest χ^2_{NC} is retained. Here NC refers to the number of constraints, which is four plus the number of two-photon π^0 and η candidates in the final state (see Table I).

TABLE I. Characteristics of the η decay channels used to reconstruct the $\psi(3686) \to \gamma\eta\pi^+\pi^-$ decays: branching fraction $\mathcal{B}$, final state topology, number of constraints (NC) in the kinematic fit, and reconstruction efficiency, ε, according to exclusive phase-space MC.

Decay	$\mathcal{B}$ [%] [2]	Final state	NC	ε [%]
$\eta \to \gamma\gamma$	39.41±0.20	3γ $1(\pi^+\pi^-)$	5	26.58
$\eta \to \pi^+\pi^-\pi^0$	22.92±0.28	3γ $2(\pi^+\pi^-)$	5	16.46
$\eta \to \pi^0\pi^0\pi^0$	32.68±0.23	7γ $1(\pi^+\pi^-)$	7	5.64
Total	95.01±0.71			16.91

A. $\chi_{c1} \to \eta\pi^+\pi^-$ event selection

The $\chi_{c1} \to \eta\pi^+\pi^-$ candidates in η three-pion decays are selected by requiring that the invariant mass of three pions satisfy:

$$0.535 < m(3\pi) < 0.560 \text{ GeV}/c^2. \quad (1)$$

For the $\eta \to \gamma\gamma$ candidates, we require that the mass constraint fit for $\eta \to \gamma\gamma$ satisfies $\chi^2_{\gamma\gamma} < 15$. The χ^2_{NC} obtained from four-momenta kinematic constraint fits are required to satisfy $\chi^2_{5C} < 40$, $\chi^2_{5C} < 40$ and $\chi^2_{7C} < 56$ for $\eta \to \gamma\gamma$, $\eta \to \pi^+\pi^-\pi^0$ and $\eta \to 3\pi^0$, respectively. To select the χ_{c1} candidates from the $\psi(3686) \to \gamma\chi_{c1}$ transition, we require the energy of the radiative photon to satisfy $0.155 < E_\gamma < 0.185$ GeV.

1. Background suppression

The major background for all final states comes from $\psi(3686) \to \eta J/\psi$, while in the $\eta \to \gamma\gamma$ case the background from $\psi(3686) \to \gamma\gamma J/\psi$ decays is also significant. The background from $\psi(3686) \to \pi\pi J/\psi$ is negligible, once a good η candidate is found.

To suppress $\psi(3686) \to \eta J/\psi$ background for all three η decays, the system recoiling against the η, with respect to the $\psi(3686)$, must have its invariant mass separated at least 20 MeV/c^2 from the J/ψ mass.

Additional selection criteria are used in the $\eta \to \gamma\gamma$ channel to suppress π^0 contamination and $\psi(3686) \to \gamma\gamma J/\psi$ production. The former background is suppressed by rejecting events in which any two-photon combination satisfies $0.110 < m(\gamma\gamma) < 0.155$ GeV/c^2. The latter background is suppressed by vetoing events for which a two-photon combination not forming an η has a total energy between 0.52 GeV $< E_{\gamma\gamma} <$ 0.60 GeV. This range of energies is associated with the doubly radiative decay $\psi(3686) \to \gamma\chi_{cJ}; \chi_{cJ} \to \gamma J/\psi$, for which the energy sum of two transitional photons is $E_{\gamma\gamma} \approx 0.560$ GeV.

2. Background subtraction

The background estimated from the inclusive MC after all selection criteria are applied is below 3% in each channel. The background from η sidebands is subtracted, and Fig. 1 shows the invariant mass distributions of η candidates with vertical dotted bars showing the η sideband regions. The sideband regions for the two-photon and three-pion modes are defined as $68 < |m(\gamma\gamma) - m_\eta| <$ 113 MeV/c^2 and $37 < |m(3\pi) - m_\eta| < 62$ MeV/c^2, respectively, where m_η is the nominal η mass [2]. In the case of η three-pion decays, the η signal region, defined by Eq. (1), is indicated by dash-dotted bars in Fig. 1. Although the mass distribution of three neutral pions, Fig. 1(c), is wider than the corresponding distribution from the charged channel, Fig. 1(b), we use the same selection criteria for both η decays, which keeps the majority of good $\eta \to 3\pi^0$ candidates and results in similar background levels in the two channels. The effects of including more data from the tails of these distributions are taken into account in the systematic uncertainties. The invariant mass plot representing $\eta \to \gamma\gamma$ candidates, Fig. 1(a), is used only to select η sidebands for background subtraction. Table I lists channel efficiencies and the effective efficiency for all channels.

The $\eta\pi^+\pi^-$ invariant mass distribution, when events from all η channels are combined, is shown on Fig. 2. In the signal region, indicated by vertical bars, there are 33919 events, with the background of 497 events estimated from the η sidebands. The sideband background does not account for all the background, and after the η-sideband background is subtracted, the remaining background is estimated by fitting the invariant mass distribution. The fit is shown by the solid black distribution, Fig. 2. For the χ_{c1} signal, a double-sided Crystal-Ball distribution (dotted) is used, and for the background, a linear function along with a Gaussian corresponding to the χ_{c2} contribution (dashed) are used. The signal purity estimated from the fit is $\mathcal{P} = (98.5 \pm 0.3)\%$, where the error is obtained from fluctuations in the background when using different fitting ranges, and shapes of the background.

B. Two-body structures in the $\chi_{c1} \to \eta\pi^+\pi^-$ decays

The Dalitz plot for selected signal events is shown in Fig. 3(a). Two-body structures reported in previous analyses of the $\chi_{c1} \to \eta\pi^+\pi^-$ decays [8, 17, 18], the $a_0(980)\pi$, $a_2(1320)\pi$ and $f_2(1270)\eta$, are indicated by the long-dash-dotted, dashed and dash-dotted arrows pointing into the Dalitz space, respectively. One feature of this distribution is the excess of events in the upper left corner of the Dalitz plot (a), pointed to by the dotted arrows, which cannot be associated with known structures observed in previous analyses of this χ_{c1} decay. We hypothesize this is due to $a_2(1700)$ production. The expected Dalitz plot of a $a_2(1700)\pi$ signal is shown in Fig. 3(b), obtained assuming that the $a_2(1700)$ is the only structure produced. The $a_2(1700) \to \eta\pi^+$ and $a_2(1700) \to \eta\pi^-$ components can not be easily identified along the dotted arrows in the Dalitz plot, Fig 3(a), but their crossing in the plot shown in Fig. 3(b) visually matches the excess of events in the upper left corner of the Dalitz plot of Fig. 3(a).

The distributions of the square of the invariant mass are shown in Fig. 3(c) for $\eta\pi$ and (d) for $\pi^+\pi^-$. Structures that correspond to $a_0(980)$, $a_2(1320)$ and $f_2(1270)$ production are evident, as well as a low-mass $\pi\pi$ peak, sometimes referred to as the σ state. In each of these two distributions there is a visible threshold effect. In the $\pi\pi$ distribution, there is a structure above the $K\bar{K}$ threshold, which is too broad to result from the $f_0(980)$ alone. In the $\eta\pi$ distribution, the broadening of the $a_0(980)$ peak around 1.2 GeV$^2/c^4$ could be associated with the $\eta'\pi$ threshold. By examining various regions in the Dalitz space, we conclude that the cross-channel contamination, or reflections, are not associated with these threshold effects in the data. In order to eliminate background as the source of these peculiar line-shapes, background studies are performed. Namely, we increased the background level by relaxing the kinematic constraint to $\chi^2_{NC}/NC < 10$ and also suppressed more background by requiring $\chi^2_{NC}/NC < 5$. In addition we varied the limits on tagging η and χ_{c1} candidates, as explained in Sec. V.

It is possible that the $\pi\pi$ line shape results from a destructive interference between the $f_0(980)$ and other

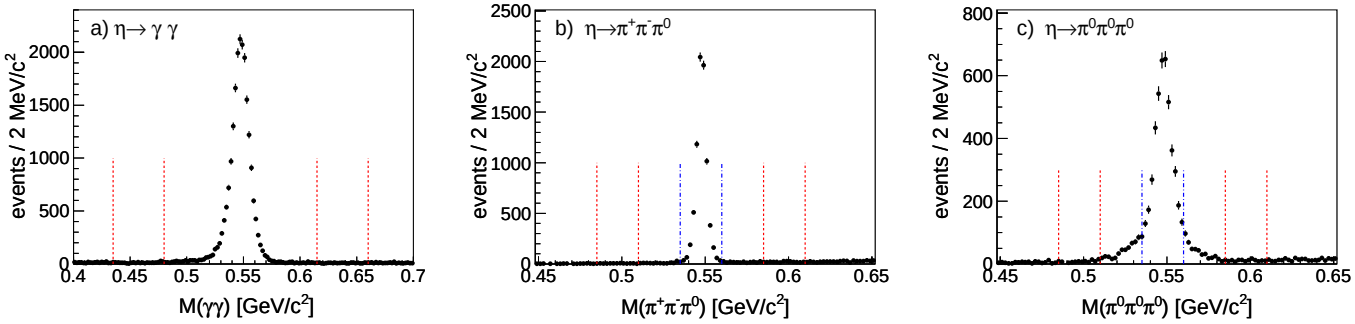

FIG. 1. The invariant mass distribution of the η candidates, where dotted (red) lines indicate regions used for background subtraction, while dash-dotted bars (blue) show η-signal boundaries for the three-pion η decay cases. There are no blue bars on plot a) since the $\eta \to \gamma\gamma$ signal is selected using the $\gamma\gamma$ kinematic constraint (color online).

components of the $\pi\pi$ S-wave. It has been known for some time that the $a_0(980) \to \eta\pi$ line shape is affected by the proximity of the $K\bar{K}$ threshold to the $a_0(980)$ mass [19]. If the $a_0(980) \to \eta'\pi$ coupling appears to be important for describing the $a_0(980) \to \eta\pi$ distribution, this would be an example when a virtual channel is influencing the distribution of another decay channel, despite its threshold being far away from the resonance peak. We use an Amplitude Analysis (AA), described in the next section, to help in answering the above questions, and to determine the nature and significance of the "crossing structure" discussed.

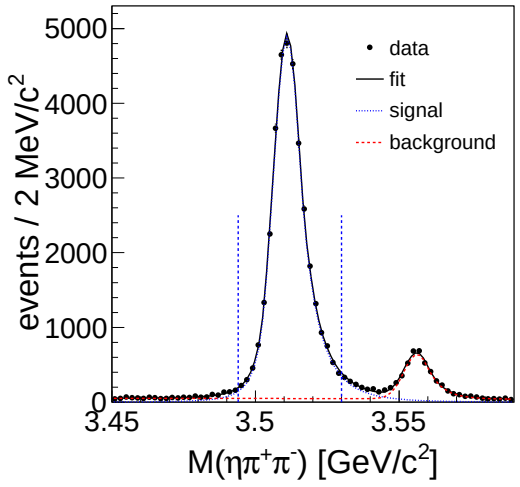

FIG. 2. Invariant mass of the χ_{c1} candidates, after the η sideband background is subtracted. Vertical bars indicate the region used to select the χ_{c1} candidates. See text for the fit discussion (color online).

III. AMPLITUDE ANALYSIS

To study the substructures observed in the $\chi_{c1} \to \eta\pi^+\pi^-$ decays, we use the isobar model, in which it is assumed that the decay proceeds through a sequence of two-body decays, $\chi_{c1} \to Rh_b$; $R \to h_1h_2$, where either an isospin-zero ($R \to \pi\pi$) or isospin-one ($R \to \eta\pi$) resonance is produced, with the total spin J, and relative orbital angular momentum L with respect to the bachelor meson, h_b. For resonances with $J > 0$, there are two possible values of L that satisfy the quantum number conservation for the $1^{++} \to (J^{PC})0^-_L$ transition.

We use the extended maximum likelihood technique to find a set of amplitudes and their production coefficients that best describe the data. The method and complete description of amplitudes constructed using the helicity formalism are given in Ref. [8], with two exceptions.

The first difference is that the events from the $\eta-$sidebands are subtracted in the likelihood function $\mathcal{L}$, with equal weight given to the left-hand and right-hand sides, using a weighting factor $\omega = -0.5$. The second difference with respect to Ref. [8] is that we deviate from the strict isobar model by allowing production amplitudes to be complex. Isospin symmetry for $\eta\pi^\pm$ resonances is imposed.

In the minimization process of the expression $-2\ln\mathcal{L}$, the total amplitude intensity, $I(\mathbf{x})$, constructed from the coherent sum of relevant amplitudes, is bound to the number of observed χ_{c1} candidates by using the integral

$$\mathcal{N}_{\chi_{c1}} = \int \xi(\mathbf{x})\mathbf{I}(\mathbf{x})\mathbf{dx}, \qquad (2)$$

where $\mathbf{x}$ represents the kinematic phase space, while $\xi(\mathbf{x})$ is the acceptance function, with the value of one (zero) for accepted (rejected) exclusive MC events. The proper normalization of different η channels is ensured by using exclusive MC samples, generated with sample sizes proportional to the η branching fractions, listed in Table I. If the complete generated exclusive MC set is used in the MC integration, then Eq. (2) provides the acceptance corrected number of χ_{c1} events, adjusted by subtracted background contributions. In this case, $\xi(\mathbf{x}) \equiv \mathbf{1}$ for all MC events. Fractional contributions, $\mathcal{F}_\alpha$, from specific amplitudes, A_α, are obtained by restricting the coherent

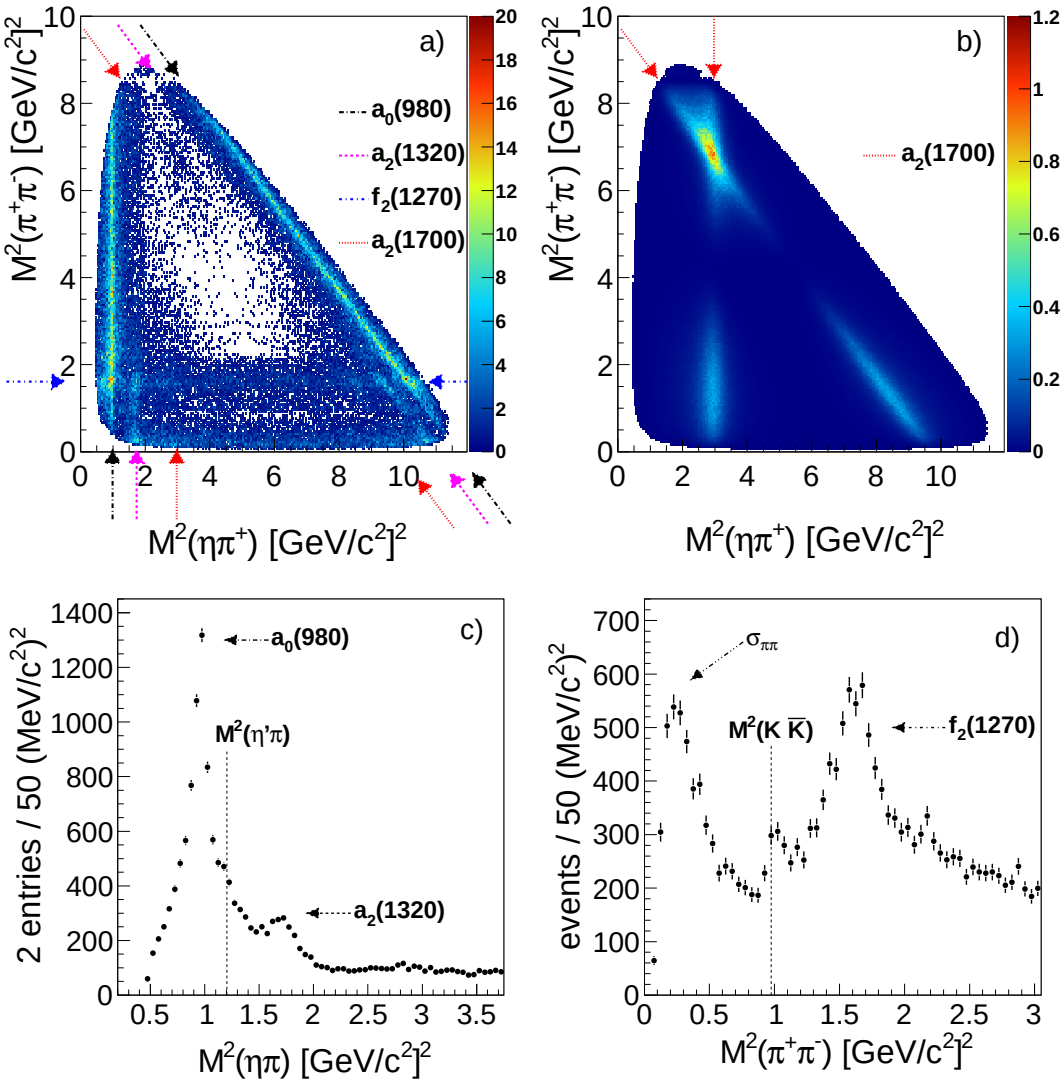

FIG. 3. Dalitz plots obtained from selected χ_{c1} candidates from (a) data and (b) exclusive MC, assuming the $a_2(1700)$ is the only structure produced. The (c) $\eta\pi$ and (d) $\pi^+\pi^-$ projections show various structures, which can also be identified by arrows in the Dalitz plot (a). Vertical dotted lines in plots (c) and (d) indicate the thresholds for producing the $\eta'\pi$ or $K\bar{K}$ in the $\eta\pi$ or $\pi\pi$ space, respectively (color online).

sum in $I(\mathbf{x})$ to $I_\alpha(\mathbf{x})$, so that

$$\mathcal{F}_\alpha = \frac{\int I_\alpha(\mathbf{x})\mathbf{dx}}{\int I(\mathbf{x})\mathbf{dx}}. \quad (3)$$

The numerator represents acceptance-corrected yield of a given substructure, used to calculate relevant branching fractions, $\mathcal{B}_\alpha$. Errors are obtained from the covariance matrix using proper error propagation, so for a given substructure, the errors on $\mathcal{B}_\alpha$ and $\mathcal{F}_\alpha$ are not necessarily the same.

The decay chain $\psi(3686) \to \gamma\chi_{c1}$; $\chi_{c1} \to \eta\pi^+\pi^-$ is described by amplitudes constructed to take into account the spin alignment of the initial state and the helicity of the radiated photon. Linear combinations of helicity amplitudes can be used to construct amplitudes in the multipole basis, matching the electric dipole ($E1$) and magnetic quadrupole ($M2$) transitions. The $\psi(3686) \to \gamma\chi_{c1}$ decay is dominated by the $E1$ transition [20], and a small $M2$ contribution ($\approx 3\%$) can be treated as a systematic uncertainity.

A. Mass dependent terms, $T_\alpha(s)$

The dependence of amplitude A_α on the energy can be separated from its angular dependence, employing a general form $p^L q^J T_\alpha(s)$, if the width of the χ_{c1} is neglected. Here, p and q are decay momenta for decays $\chi_{c1} \to R_J h_b$ and $R_J \to h_1 h_2$ in the rest frame of the χ_{c1}

and a resonance R_J, respectively, while $s = m_{12}^2$ is the squared invariant mass of the corresponding isobar products ($\pi\pi$ or $\eta\pi$). For most resonances, we use relativistic Breit-Wigner (BW) distributions, with spin-dependent Blatt-Weisskopf factors [21]. For the $a_0(980)$ and $\pi\pi$ S-wave line shapes, we use different prescriptions explained below.

To account for the non-resonant process $\chi_{c1} \to \eta\pi^+\pi^-$, we use an amplitude constructed as the sum of all possible final state combinations of helicity amplitudes constrained to have the same production strength, with no dependence on the invariant mass of the respective two-body combinations.

1. *Parametrization of* $a_0(980)$

Instead of using the usual Flatté formula [19] to describe the $a_0(980)$ line-shape, we use dispersion integrals, following the prescription given in Ref. [12]. We consider three $a_0(980)$ decay channels, the $\eta\pi$, $K\bar{K}$, and $\eta'\pi$, with corresponding coupling constants, g_{ch}, and use an appropriate dispersion relation to avoid the problem of a false singularity [22] present in the $\eta'\pi$ mode (see discussion at the end of this section). The $a_0(980)$ amplitude is constructed using the following denominator:

$$D_\alpha(s) = m_0^2 - s - \sum_{ch} \Pi_{ch}(s), \tag{4}$$

where m_0 is the $a_0(980)$ mass and $\Pi_{ch}(s)$ in the sum over channels is a complex function, with imaginary part

$$\mathrm{Im}\Pi_{ch}(s) = g_{ch}^2 \rho_{ch}(s) F_{ch}(s), \tag{5}$$

while real parts are given by principal value integrals

$$\mathrm{Re}\Pi_{ch}(s) = \frac{1}{\pi} P \int_{s_{ch}}^{\infty} \frac{\mathrm{Im}\Pi_{ch}(s')ds'}{(s'-s)}. \tag{6}$$

In the above expressions $\rho_{ch}(s)$ is the available phase space for a given channel, obtained from the corresponding decay momentum $q_{ch}(s)$: $\rho_{ch}(s) = 2q_{ch}(s)/\sqrt{s}$. The integral in Eq. (6) is divergent when $s \to \infty$, so the phase space is modified by a form factor $F_{ch}(s) = e^{-\beta q_{ch}^2(s)}$, where the parameter β is related to the root-mean-square (RMS) size of an emitting source [12]. We use $\beta = 2.0$ $[\mathrm{GeV}/c^2]^{-2}$ corresponding to RMS = 0.68 fm, and we verify that our results are not sensitive to the value of β. The integration in Eq. (6) starts from the threshold for a particular channel, s_{ch}, which conveniently solves the problem of the analytical continuation in special cases of final state configurations like the $a_0(980) \to \eta'\pi$, when the decay momentum below the threshold ($s < m_{\eta'} + m_\pi$) becomes real again for $s < m_{\eta'} - m_\pi$. Figure 4 shows the shapes of (a) $\mathrm{Im}\Pi_{ch}(s)$ and (b) $\mathrm{Re}\Pi_{ch}(s)$ (b), for the $K\bar{K}$ and $\eta'\pi$ channels, for arbitrary values of the coupling constants. In the final form, the real parts in the denominator of Eq. (4) are adjusted by $\mathrm{Re}\Pi_{ch}(m_0)$ terms: $\mathrm{Re}\Pi_{ch}(s) \to \mathrm{Re}\Pi_{ch}(s) - \mathrm{Re}\Pi_{ch}(m_0)$.

2. $\pi\pi$ S-*wave model*

The $\pi\pi$ S-wave parametrization follows the prescription given in Ref. [8], in which two independent processes for producing a $\pi\pi$ pair are considered: direct $(\pi\pi)_S \to (\pi\pi)_S$, and production through kaon loops, $(K\bar{K})_S \to (\pi\pi)_S$. Amplitudes corresponding to these scattering processes, labeled $S_{\pi\pi}(s)$ and $S_{K\bar{K}}(s)$, are based on di-pion phases and intensities obtained from scattering data [23], which cover the $\pi\pi$ invariant mass region up to 2 GeV/c^2. The $S_{\pi\pi}(s)$ component is adapted in Ref. [8] to account for differences in the $\pi\pi$ production through scattering and decay processes, using the denominator, $D(s)$, extracted from scattering experiments. The $S_{\pi\pi}(s)$ amplitude in this analysis takes the form:

$$S_{\pi\pi}(s) = c_0 S^0(s) + \sum_{i=1} c_i z^i_{s_{K\bar{K}}}(s) S^0(s) + \sum_{i=1} c'_i z^i_{s'}(s) S^0(s). \tag{7}$$

The common term in the above expression, $S^0(s) = 1/D(s)$, is expanded using conformal transformations of the type

$$z_{s_{\rm th}}(s) = \frac{\sqrt{s+s_0} - \sqrt{s_{\rm th}-s}}{\sqrt{s+s_0} + \sqrt{s_{\rm th}-s}}, \tag{8}$$

which is a complex function for $s > s_{th}$. Equation (7) features two threshold-functions, $z_{s_{\rm th}}(s)$, one corresponds to $K\bar{K}$ production with $s_{K\bar{K}} = 4m_K^2$, while another with $s_{\rm th} = s'$ could be used to examine other possible threshold effects in di-pion production. The c_i, $i = 1, 2$ are production coefficients to be determined.

Figure 5 shows the (a) phase and (b) intensity of various components used in constructing the $\pi\pi$ S-wave amplitude based on two functions given by Eq. (8), with different thresholds: $z_{K\bar{K}}(s)$ and $z_{s'}(s)$. The following convention is used: $S^i_{\pi\pi}(s) = z^i_{K\bar{K}} S^0(s)$, $S'^i_{\pi\pi}(s) = z^i_{s'} S^0(s)$. Components are arbitrarily scaled, and we set $\sqrt{s'} \sim 1500$ MeV/c^2, similarly to the value used later in analysis. The parameter $s_0 = 1.5$ $(\mathrm{GeV}/c^2)^2$ can be used to adjust the left-hand cut in the complex plane, and the same value is used in all components.

IV. RESULTS

We present results from the amplitude analysis of the full decay $\psi(3686) \to \gamma\chi_{c1}$; $\chi_{c1} \to \eta\pi^+\pi^-$, reconstructed in three major η decay modes. The optimal solution to describe the data is found by using amplitudes with fractional contributions larger than 0.5% and significance larger than 5σ. The significance for each amplitude α is determined from the change in likelihood with respect to the null-hypothesis, $\Delta\Lambda = -2\ln\mathcal{L}_0/\mathcal{L}_\alpha$. The null-hypothesis for a given amplitude is found by excluding it from the base-line fit, and the corresponding amplitude significance is calculated taking into account the change

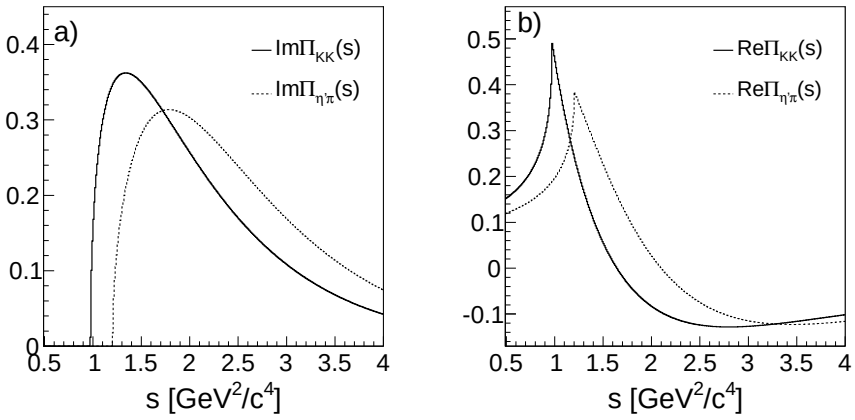

FIG. 4. Line shapes of (a) $\mathrm{Im}\Pi(s)$ and (b) $\mathrm{Re}\Pi(s)$ for the $K\bar{K}$ and $\eta'\pi$ production with arbitrary normalization.

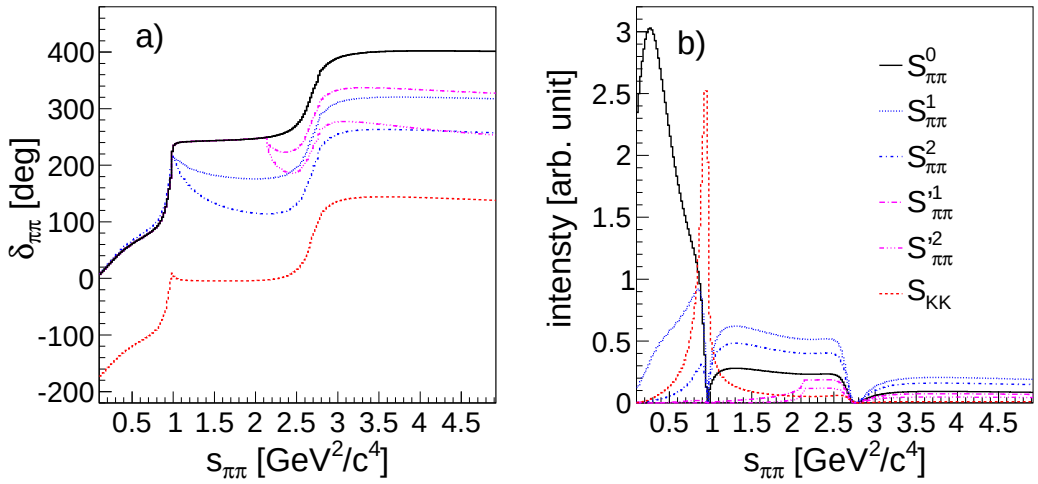

FIG. 5. The (a) phase and (b) intensity of the $\pi\pi$ S-wave components. Red (dash) histograms represent the $S_{K\bar{K}}$ amplitude, blue histograms (dot and dash-dot) are obtained using $S^i_{\pi\pi} = z^i_{K\bar{K}} S^0_{\pi\pi}$ terms, while purple (long-dash-dot and dash-three-dot) represent $S'^i_{\pi\pi} = z^i_{s'} S^0_{\pi\pi}$ terms (color online).

in the number of degrees of freedom, which is two (four) for $J = 0$ ($J > 0$) amplitudes.

The most dominant amplitude in this reaction is $a_0(980)\pi$, as evident from the $\eta\pi$ projection of the Dalitz plot, Fig. 3(c). Other amplitudes used in our baseline fit include the $S_{K\bar{K}}\eta$, $S_{\pi\pi}\eta$, $f_2(1270)\eta$, $f_4(2050)\eta$, $a_2(1320)\pi$ and $a_2(1700)\pi$, where masses and widths of resonances described by BW functions are taken from the PDG [2], while the $a_2(1700)$ and $a_0(980)$ parameters are free parameters to be determined by the fit in this work. The mass projections are shown in Fig. 6, and the corresponding fractional contributions and significances are listed in Table II. For amplitudes with spin $J > 0$ both orbital momentum components are included.

The following components form the $S_{\pi\pi}(s)$ amplitude:

$$S_{\pi\pi}(s) = c_0 S^0(s) + c_1 S^1_{\pi\pi}(s) + c'_1 S'^1_{\pi\pi}(s) + c'_2 S'^2_{\pi\pi}(s). \quad (9)$$

As indicated earlier, the threshold used to construct the $S^1(s)$ term is $s_{K\bar{K}} = 4m^2_K$. The threshold for the $S'^i(s)$ components ($i = 1, 2$) is $s' = 2.23$ [GeV/c^2]^2, which is close to the mass of the $f_0(1500)$, and it is responsible for the peaking of the $S_{\pi\pi}\eta$ amplitude in this region, Fig. 6(b). In fact, the $S'^i(s)$ components are used instead of the $f_0(1500)\eta$ amplitude, which would be needed in the optimal solution if only threshold functions $z^i_{K\bar{K}}(s)$ were used in the expansion of the $S_{\pi\pi}(s)\eta$ amplitude. With these additional terms, the contribution and significance of $\pi\pi$ scalars, the $f_0(1370)$, $f_0(1500)$ and $f_0(1710)$, is negligible, for each. Although this particular set of amplitudes respects the unitarity of the $\pi\pi$ S-wave, we use the sum of BW to model other spins and final states, namely the $f_2(1270)$, $f_4(2050)$, $a_2(1320)$ and $a_2(1700)$. Our approach provides reasonable modeling of the $\pi\pi$ line shape, and the sum of all $\pi\pi$ S-wave components, $S_{K\bar{K}}$ and $S_{\pi\pi}$, is reported in Table II.

Besides the $f_0(1370)$, $f_0(1500)$, and $f_0(1710)$, other

conventional resonances are probed, including the $f_0(1950)$, $f_2(1525)$, $f_2(2010)$, and $a_0(1450)$, with parameters fixed to PDG values [2]. They do not pass the tests for significance and fractional contribution. The non-resonant $\chi_{c1} \to \eta\pi^+\pi^-$ production is found to be negligible. The search for possible 1^{-+} resonances in the $\eta\pi$ final state will be presented below.

A. The $a_2(1700)$ signature

All structures listed in Table II have been already reported in the decay $\chi_{c1} \to \eta\pi^+\pi^-$, except the $a_2(1700)\pi$. Its fractional contribution is around 1%, and the significance of each orbital momentum component is more than 10σ. Detailed background studies are performed to ensure that the background, remaining after η-sideband subtraction, is not affecting the significance and fractional contribution of the $a_2(1700)$. Results of fitting the mass and width of the $a_2(1700)$, shown in Table III, are consistent with the values listed by the PDG [2]. To check how the $a_2(1700)$ parameters and fractional contributions are affected by the $f_2(1270)$ and $a_2(1320)$, we also fitted their masses and widths, which are provided in Table III with statistical uncertainties only. The mass (width) of the $f_2(1270)$ is lower (higher) than its nominal value [2], maybe because of interference with underlying $\pi\pi$ S-wave components or threshold effects, other than those for the $K\bar{K}$ or $f_0(1500)$ production.

The systematic uncertainties for the $a_2(1700)$ mass and width are obtained by varying parameters of other amplitudes within respective uncertainties listed in Ref. [2], and taking into account variations listed in Table III. The $a_0(980)$ errors are shown in Table IV. Variations in the shape of the $\pi\pi$-S wave amplitude are taken into account by changing terms in the expansion, Eq. (9).

We also test the significance of the $a_2(1700)$ including alternative states with the same mass and width, but different spins: $J = 0, 1, 4$. In all cases, the significance of the $a_2(1700)$ in the presence of an alternative state exceeds 17σ. The statistical significance of the $a_2(1700)$ signal alone is 20σ. This result confirms our hypothesis based on a visual inspection of the Dalitz plot, Fig. 3(a), that the excess of events in the upper left corner of the Dalitz space results from the $a_2(1700)$ production, and it is associated with the crossing of the $a_2(1700)^+\pi^-$ and $a_2(1700)^-\pi^+$ components.

B. $a_0(980)$ parameters

When determining the $a_0(980)$ parameters we use the ratios $R_{21} = g^2_{K\bar{K}}/g^2_{\eta\pi}$, and $R_{31} = g^2_{\eta'\pi}/g^2_{\eta\pi}$. The resulting values are listed in Table IV, where systematic uncertainties are obtained by fitting the $a_0(980)$ parameters under different conditions. The level of background is varied by changing selection criteria described in Sec. II, and by changing the amount of background subtracted from the η sidebands. Effects of the line shapes of the $a_2(1320)$, $a_2(1700)$, $f_2(1270)$ and $f_4(2050)$ resonances are taken into account by varying their masses and widths within the respective uncertainties [2], and using values from Table III. The effect of the $\pi\pi$ S-wave shape is examined in similar way as for the $a_2(1700)$. The presence of alternative conventional and exotic resonances is also taken into account. Our result is not sensitive to the value of the parameter β in Eqs. (5) and (6), within the range of values: $\beta = (2.0 \pm 1.0)$ [GeV/c^2]^2.

For comparison we list two previous results, one from a similar experiment, CLEO-c, and the other obtained using Crystal Barrel data. There is a general agreement between different analyses for the $a_0(980)$ mass and R_{21}. The ratio R_{31} was fixed in Ref. [12] to the theoretical value provided by Eq.(11), while it was consistent with zero in the CLEO-c analysis, possibly because of smaller statistics. It is not easy to comment on the difference in values for the $\eta\pi$ coupling, which could be affected by different normalizations used by different analyses.

This analysis provides the first non-zero measurement of the coupling constant $g_{\eta'\pi}$. To test the sensitivity of the $a_0(980) \to \eta\pi$ line shape to the decay $a_0(980) \to \eta'\pi$, we repeat the analysis with $g_{\eta'\pi} = 0$, and let the values of the other parameters free. The results of this fit are also given in Table IV. The likelihood change when the $\eta'\pi$ channel is ignored shows that the significance of a non-zero $g_{\eta'\pi}$ measurement is 8.9σ. The same result is obtained when the analysis is performed in the presence of the $a_0(1450)$. The values of the two ratios based on the SU(3) expectation are

$$g^2_{K\bar{K}}/g^2_{\eta\pi} = 1/(2\cos^2\phi) = 0.886 \pm 0.034, \qquad (10)$$

$$g^2_{\eta'\pi}/g^2_{\eta\pi} = \tan^2\phi = 0.772 \pm 0.068, \qquad (11)$$

which depend on the choice of the η–η' mixing angle; $\phi = (41.3 \pm 1.2)^\circ$ in this case [12]. Our result is consistent with Eq. (11) within 1.5σ, based on the quoted uncertainties.

C. Search for $\eta\pi$ P-wave states

We examine possible exotic meson production in the $\eta\pi$ invariant mass region from 1.4 to 2.0 GeV/c^2. Table II lists fractional contributions and significances of three $J^{PC} = 1^{-+}$ candidates, added one at the time to our nominal fit. Two possible orbital-momentum configurations for an exotic amplitude are the S-wave and D-wave, and the significance of each is tested individually. We find that the significance of the S-wave is marginal, less than 2σ for every π_1, and the reported significances in Table II result from using the S and D waves together in the fit. The most significant of the three possible exotic states is the $\pi_1(1400)$, with a significance of 3.5σ

TABLE II. Fractional intensities $\mathcal{F}$, and significances of amplitudes in the base-line fit, with the first and second errors being statistical and systematic, respectively. The third error for the branching fractions for the $\chi_{c1} \to \eta\pi^+\pi^-$ decay and decays into significant conventional isobars is external (see text). For exotic mesons only statistical errors on their fractional contributions are provided. The upper limits for exotic meson candidates, which include both statistical and systematic uncertainties, are at the 90% confidence-level. The coherent sum of all $\pi\pi$ S-wave components, $(\pi^+\pi^-)_S\eta$, is included in this report. Note, the branching fractions for amplitudes of the type $A_\alpha\eta$, involving isobars decaying into $\pi^+\pi^-$, are the products of $\chi_{c1} \to A_\alpha\eta$ and $A_\alpha \to \pi^+\pi^-$ rates. Branching fractions for isobars decaying into $\eta\pi$ include charge conjugates.

Decay	$\mathcal{F}$ [%]	Significance [σ]	$\mathcal{B}(\chi_{c1} \to \eta\pi^+\pi^-)$ [10^{-3}]
$\eta\pi^+\pi^-$	-	-	4.67 ± 0.03 ± 0.23 ± 0.16
$a_0(980)^+\pi^-$	72.8 ± 0.6 ± 2.3	> 100	3.40 ± 0.03 ± 0.19 ± 0.11
$a_2(1320)^+\pi^-$	3.8 ± 0.2 ± 0.3	32	0.18 ± 0.01 ± 0.02 ± 0.01
$a_2(1700)^+\pi^-$	1.0 ± 0.1 ± 0.1	20	0.047 ± 0.004 ± 0.006 ± 0.002
$S_{K\bar{K}}\eta$	2.5 ± 0.2 ± 0.3	22	0.119 ± 0.007 ± 0.015 ± 0.004
$S_{\pi\pi}\eta$	16.4 ± 0.5 ± 0.7	> 100	0.76 ± 0.02 ± 0.05 ± 0.03
$(\pi^+\pi^-)_S\eta$	17.8 ± 0.5 ± 0.6	-	0.83 ± 0.02 ± 0.05 ± 0.03
$f_2(1270)\eta$	7.8 ± 0.3 ± 1.1	> 100	0.36 ± 0.01 ± 0.06 ± 0.01
$f_4(2050)\eta$	0.6 ± 0.1 ± 0.2	9.8	0.026 ± 0.004 ± 0.008 ± 0.001
Exotic candidates			U.L. [90% C.L.]
$\pi_1(1400)^+\pi^-$	0.58±0.20	3.5	< 0.046
$\pi_1(1600)^+\pi^-$	0.11±0.10	1.3	< 0.015
$\pi_1(2015)^+\pi^-$	0.06±0.03	2.6	< 0.008

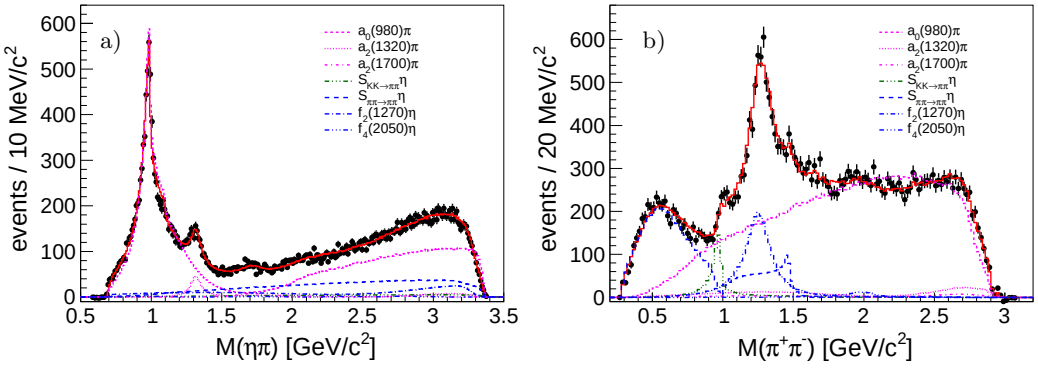

FIG. 6. Projections in the (a) $\eta\pi$ and (b) $\pi^+\pi^-$ invariant mass from data, compared with our base-line fit (solid curve) and corresponding amplitudes (various dashed and dotted lines). All features of the data, including structures discussed in Sec. II B are reproduced rather well.

and fractional contribution less than 0.6%. Masses and widths of the three exotic candidates are not very well constrained by previous analyses, and we vary the respective parameters within listed limits [2]. Our conclusion is that there is no significant evidence for an exotic $\eta\pi$ structure in the $\chi_{c1} \to \eta\pi^+\pi^-$ decays, and we determine upper limits at the 90% confidence level for the production of each π_1 candidate.

D. Branching fractions

The branching fraction for the $\chi_{c1} \to \eta\pi^+\pi^-$ decay is given by

$$\mathcal{B}(\chi_{c1} \to \eta\pi^+\pi^-) = \frac{\mathcal{P} * \mathcal{N}_{\chi_{c1}\to\eta\pi^+\pi^-}}{N_{\psi(3686)} B_{\psi(3686)\to\gamma\chi_{c1}} B_\eta \epsilon}, \quad (12)$$

where the branching fractions $B_{\psi(3686)\to\gamma\chi_{c1}}$ and B_η are from Ref. [2]; the latter is listed in Table I. The number of $\psi(3686)$, $N_{\psi(3686)}$, [14, 15] is provided in Sec II. The signal purity, $\mathcal{P}$, given in Sec. II A 1, takes into account that the number of χ_{c1} obtained from the amplitude analysis includes the background not accounted for by the sideband subtraction. Using Eq. (2) we obtain $\mathcal{N}_{\chi_{c1}} = 192658 \pm 1075$, where the error is from the covariance matrix. The efficiency in Eq. (12) is $\epsilon \equiv 1$, by construction.

Table II lists the branching fraction for the $\chi_{c1} \to \eta\pi^+\pi^-$, and branching fractions for subsequent resonance production in respective isospin states, $\eta\pi^\pm$ or $\pi^+\pi^-$, where the first and second errors are statistical and systematic, respectively. The branching fraction for

TABLE III. The mass and width of the $a_2(1700)$, with statistical and systematic uncertainties. Only statistical uncertainties from the $f_2(1270)$ and $a_2(1320)$ fits are listed. Comparison with the PDG [2] values is provided, with all units in GeV/c^2.

	BESIII		PDG [2]	
Resonance	M	Γ	M	Γ
$a_2(1700)$	1.726±0.012±0.025	0.190±0.018±0.030	1.732±0.016	0.194±0.040
$f_2(1270)$	1.258±0.003	0.206±0.008	1.275±0.001	0.185±0.003
$a_2(1320)$	1.317±0.002	0.090±0.005	1.318±0.001	0.107±0.005

TABLE IV. Parameters of the $a_0(980)$ determined from the fit using the dispersion relation of Eqs. (4-6), compared to results from previous analyses. Bold values indicate quantities that are fixed in the fit.

Data	m_0 [GeV/c^2]	$g^2_{\eta\pi}$ [GeV/c^2]^2	$g^2_{K\bar{K}}/g^2_{\eta\pi}$	$g^2_{\eta'\pi}/g^2_{\eta\pi}$
CLEO-c [8]	0.998 ± 0.016	0.36 ± 0.04	0.872 ± 0.148	0.00 ± 0.17
C.Barrel [12]	0.987 ± 0.004	0.164 ± 0.011	1.05 ± 0.09	**0.772**
BESIII	0.996±0.002±0.007	0.368±0.003±0.013	0.931±0.028±0.090	0.489±0.046±0.103
BESIII ($R^2_{31} \equiv 0$)	0.990±0.001	0.341±0.004	0.892±0.022	**0.0**

a given substructure is effectively a product:

$$\mathcal{B}_\alpha = \mathcal{F}_\alpha \times \mathcal{B}(\chi_{c1} \to \eta\pi^+\pi^-), \tag{13}$$

obtained using generated exclusive MC in accordance with Eq. (3). The third error is external, associated with uncertainties in the branching fractions for the radiative transition $\psi(3686) \to \gamma\chi_{c1}$ and η decays. We also show the total $\pi^+\pi^-$ S-wave contribution, obtained from the coherent sum of the $S_{K\bar{K}}$ and $S_{\pi\pi}$ components. Statistical errors, as well as systematic ones, for a given fractional contribution and branching fraction differ, because common systematic uncertainties for all amplitudes cancel when fractions are calculated, which will be discussed below.

The upper limits for the production of the $\pi_1(1400)\pi$, $\pi_1(1600)\pi$, and $\pi_1(2015)\pi$ are shown in Table II. The limits are determined by including the corresponding amplitude in the nominal fit, one at a time. The analysis is repeated by changing other amplitude line shapes, and the background level, in a similar fashion used for determining systematic uncertainties of nominal amplitudes (see Sec. V). Masses and widths of exotic candidates are also varied within limits provided by the PDG [2]. The largest positive deviation of the exotic candidate yield with respect to the corresponding yield from the modified nominal fit is effectively treated as the systematic error, summed in quadrature with the statistical error on a given exotic state yield. The resulting uncertainty is used to determine the 90% confidence level deviation, and added to the 'nominal' yield of an exotic candidate to obtain the corresponding upper limit for the branching fraction $B(\chi_{c1} \to \pi_1^+\pi^-)$.

The branching fractions for the substructures in $\chi_{c1} \to \eta\pi^+\pi^-$ decays reported by the PDG [2] are compared in Table V with the values measured in this work, and with the previous most precise measurement (CLEO-c) [8]. The measurement for the $f_2(1270)$ production is adjusted to account for the measured relative $f_2(1270) \to \pi^+\pi^-$ width. There is a rather large discrepancy between the values for the two most dominant substructures listed by the PDG and the two most recent measurements. There is very good agreement between the last two measurements, suggesting that the PDG values on two-body structures observed in $\chi_{c1} \to \eta\pi^+\pi^-$ need to be updated.

TABLE V. Comparison between recent measurements of the branching fractions $B(\chi_{c1} \to \eta\pi^+\pi^-)$, and with the PDG values.

	$\mathcal{B}(\chi_{c1} \to \eta\pi^+\pi^-) \times[10^{-3}]$		
Decay	BESIII	CLEO-c [8]	PDG [2]
$\eta\pi^+\pi^-$	4.67 ± 0.28	4.97 ± 0.31	4.9 ± 0.5
$a_0(980)^+\pi^-$	3.40 ± 0.23	3.29 ± 0.22	1.8 ± 0.6
$f_2(1270)\eta$	0.64 ± 0.11	0.66 ± 0.11	2.7 ± 0.8

V. SYSTEMATIC UNCERTAINTIES

Tables VI summarizes various contributions to the systematic uncertainties in determining the $\chi_{c1} \to \eta\pi^+\pi^-$ branching fraction, and Table VII shows the systematics on the fractional contributions of amplitudes in the nominal fit. Systematic uncertainties in determining the $\chi_{c1} \to \eta\pi^+\pi^-$ branching fraction stem from uncertainties in charged track and shower reconstruction efficiencies, the contribution of the $M2$ multipole transition, amplitude modeling, the background contribution, and the uncertainty in the number of $\psi(3686)$ produced at

BESIII [14, 15]. External sources of uncertainty include the branching fraction $B(\psi(3686) \to \gamma\chi_{c1})$ and the fraction of η decays, $B(\eta)$ in Eq. (12). The external error affects only branching fractions, not fractional contributions, and it is reported as a separate uncertainty.

Systematic uncertainties associated with the tracking efficiency and shower reconstruction are 1% per track and 1% per photon. Because of different final states used in this analysis, tracking and photon uncertainties are weighted according to the product of branching fractions and efficiencies of the different η channels, as listed in Table I. The resulting systematic uncertainties for charged tracks and photons are 2.47% and 3.92%, respectively.

The electromagnetic transition $\psi(3686) \to \gamma\chi_{c1}$ is dominated by the $E1$ multipole amplitude with a small fraction of the $M2$ transition [20]. The nominal fit takes only the $E1$ multipole amplitude. Adding a small contribution of the $M2$ helicity amplitude, of 2.9%, we find a difference in the branching fraction of 0.62%. This is taken as a systematic uncertainty.

When considering the effects of modeling line-shapes of different amplitudes, we repeat the analysis changing the mass and width of resonances, $a_2(1320)$, $f_2(1270)$, and $f_4(2050)$, within respective uncertainties, and change the $a_0(980)$ and $a_2(1700)$ parameters within the limits of their statistical uncertainties, given in Tables IV and III. We also change BW line shapes by replacing spin-depend widths with fixed widths, and take into account the χ_{c1} width and centrifugal-barrier as another systematic error. The largest effect from all these sources is taken as a systematic uncertainty for the branching fractions and fractional contributions.

The effect of background is estimated by varying the kinematic-constraint requirement, changing limits on tagging η and χ_{c1} candidates, changing the level of suppression of the J/ψ and π^0 productions, and the level of background subtraction. As a general rule, selection criteria were changed to allow for $\approx 1\sigma$ additional background events, based on the numbers from the inclusive MC. We use $\chi^2_{NC}/NC < 9$ in all three modes when varying the kinematic constraint. To select χ_{c1} candidates, we use photon energy ranges of (0.152-0.187) GeV, in the $\eta \to \gamma\gamma$ channel, and (0.150-0.190) GeV, in two $\eta \to 3\pi$ channels. The mass window for the η selection is changed to (0.530-0.565) GeV/c^2. The π^0 suppression window is reduced to (0.120-0.150) GeV/c^2 and the J/ψ suppression is reduced by vetoing two-photon energy within (0.525-0.595) GeV. We also determine the branching fractions without background subtraction from η-sidebands, and the largest effect is listed in Tables VI and VII.

Some uncertainties that are common for all amplitudes, like tracking, shower reconstruction, and $N_{\psi(3686)}$ errors, cancel out in the fractional contributions. However, they are taken into account when branching fractions are determined.

TABLE VI. Systematic uncertainties in determining the branching fraction $B(\chi_{c1} \to \eta\pi^+\pi^-)$. The systematic uncertainty per track is 1.0%, and for photons it is 1.0% per shower.

Contribution	Relative uncertainty (%)
MDC tracking	2.5
photon detection	3.9
$M2/E1$	0.6
Background	1.6
Amplitude modeling	0.1
$N_{\psi(3686)}$	0.7
Total	5.0
External	3.4

TABLE VII. Systematic uncertainties in fractional contributions, in percent, for the base-line amplitudes used to model the $\chi_{c1} \to \eta\pi^+\pi^-$ decays.

Source	$M2/E1$	Bckg.	$T_\alpha(s)$	Total
$a_0(980)\pi$	0.2	0.5	3.1	3.2
$a_2(1320)\pi$	0.5	5.6	5.6	7.9
$a_2(1700)\pi$	1.4	3.8	12	13
$S_{kk}\eta$	3.7	2.2	11	11.5
$S_{pp}\eta$	1.1	1.1	4.3	4.6
$\pi\pi_S\eta$	1.5	1.1	3.0	3.6
$f_2(1270)\eta$	0.5	2.3	14	15
$f_4(2050)\eta$	5.6	25	18	32

VI. SUMMARY

We analyze the world's largest $\chi_{c1} \to \eta\pi^+\pi^-$ sample, selected with very high purity, and find a very prominent $a_0(980)$ peak in the $\eta\pi^\pm$ invariant mass distribution. An amplitude analysis of the $\psi(3686) \to \gamma\chi_{c1}$; $\chi_{c1} \to \eta\pi^+\pi^-$ decay is performed, and the parameters of the $a_0(980)$ are determined using a dispersion relation. The $a_0(980)$ line shape in its $\eta\pi$ final state appears to be sensitive to the details of the $a_0(980) \to \eta'\pi$ production, and for the first time, a significant non-zero coupling of the $a_0(980)$ to the $\eta'\pi$ mode is measured with a statistical significance of 8.9σ.

We also report $a_2(1700)\pi$ production in the $\chi_{c1} \to \eta\pi^+\pi^-$ decays for the first time, with the mass and width in agreement with world average values, and this analysis provides both qualitative and quantitative evidence for the existence of the $a_2(1700)$. First, the signature of the $a_2(1700)$ in the Dalitz space is consistent with the observed Dalitz plot distribution. Second, the $a_2(1700)$ significance from the amplitude analysis is larger than 17σ, compared to alternative spin assignments, even though the fractional yield of the $a_2(1700)\pi$ is only 1%. This may help in listing the $a_2(1700)$ as an established resonance by the the PDG [2].

We examine the production of exotic mesons that might be expected in the $\chi_{c1} \to \eta\pi\pi$ decays: the $\pi_1(1400)$, $\pi_1(1600)$ and $\pi_1(2015)$. There is only weak evidence for the $\pi_1(1400)$ while other exotic candidates are only marginally significant, and we determine the upper limits on the respective branching fractions.

ACKNOWLEDGMENTS

The BESIII collaboration thanks the staff of BEPCII and the IHEP computing center for their strong support. This work is supported in part by National Key Basic Research Program of China under Contract No. 2015CB856700; National Natural Science Foundation of China (NSFC) under Contracts Nos. 11235011, 11322544, 11335008, 11425524; the Chinese Academy of Sciences (CAS) Large-Scale Scientific Facility Program; the CAS Center for Excellence in Particle Physics (CCEPP); the Collaborative Innovation Center for Particles and Interactions (CICPI); Joint Large-Scale Scientific Facility Funds of the NSFC and CAS under Contracts Nos. U1232201, U1332201; CAS under Contracts Nos. KJCX2-YW-N29, KJCX2-YW-N45; 100 Talents Program of CAS; National 1000 Talents Program of China; INPAC and Shanghai Key Laboratory for Particle Physics and Cosmology; Istituto Nazionale di Sic Nucleare, Italy; Joint Large-Scale Scientific Facility Funds of the NSFC and CAS under Contract No. U1532257; Joint Large-Scale Scientific Facility Funds of the NSFC and CAS under Contract No. U1532258; Koninklijke Nederlandse Akademie van Wetenschappen (KNAW) under Contract No. 530-4CDP03; Ministry of Development of Turkey under Contract No. DPT2006K-120470; The Swedish Resarch Council; U. S. Department of Energy under Contracts Nos. DE-FG02-05ER41374, DE-SC-0010504, de-sc0012069; U.S. National Science Foundation; University of Groningen (RuG) and the Helmholtzzentrum fuer Schwerionenforschung GmbH (GSI), Darmstadt; WCU Program of National Research Foundation of Korea under Contract No. R32-2008-000-10155-0

[1] C. A. Meyer and E. S. Swanson. *Prog. Part. Nucl. Phys.*, 82:21, 2015.
[2] K. Olive et al. *Chin. Phys.*, C38:090001, 2015.
[3] D. Alde et al. *Phys. Lett.*, B205:397, 1988.
H. Aoyagi et al. *Phys. Lett.*, B314:246, 1993.
[4] A. Abele et al. *Phys. Lett.*, B423:175, 1998.
A. Abele et al. *Phys. Lett.*, B446:349, 1999.
[5] G. S. Adams et al. *Phys. Lett.*, B657:27, 2007.
[6] Alexander Donnachie and Philip R. Page. *Phys. Rev.*, D58:114012, 1998.
Adam P. Szczepaniak, Maciej Swat, Alex R. Dzierba, and Scott Teige. *Phys. Rev. Lett.*, 91:092002, 2003.
[7] Yu. A. Khokhlov. *Nucl. Phys.*, A663:596, 2000.
E. I. Ivanov et al. *Phys. Rev. Lett.*, 86:3977, 2001.
[8] G. S. Adams et al. *Phys. Rev.*, D84:112009, 2011.
[9] Robert L. Jaffe. *Phys. Rev.*, D15:267, 1977.
F. E. Close, Nathan Isgur, and S. Kumano. *Nucl. Phys.*, B389:513, 1993.
[10] N. N. Achasov and V. N. Ivanchenko. *Nucl. Phys.*, B315:465, 1989.
[11] S. Teige et al. *Phys. Rev.*, D59:012001, 1999.
[12] D. V. Bugg. *Phys. Rev.*, D78:074023, 2008.
[13] Claude Amsler et al. *Eur. Phys. J.*, C23:29, 2002.
Kazuo Abe et al. *Eur. Phys. J.*, C32:323, 2003.
[14] M. Ablikim et al. *Chin. Phys.*, C37:063001, 2013.
[15] Using the same method as in ref [14], the number of $\psi(3686)$ from the 2012 run period is found to be $(341.1 \pm 2.0) \times 10^6$, in preparation for publication.
[16] M. Ablikim et al. *Nucl. Instrum. Meth.*, A614:345, 2010.
[17] M. Ablikim et al. *Phys. Rev.*, D74:072001, 2006.
[18] S. B. Athar et al. *Phys. Rev.*, D75:032002, 2007.
[19] S. M. Flatte. *Phys. Lett.*, B63:224, 1976.
[20] M. Artuso et al. *Phys. Rev.*, D80:112003, 2009.
[21] J. M. Blatt and V. F. Weisskopf. *Theoretical Nuclear Physics*. Wiley, NewYork, 1951.
[22] V. V. Anisovich and A. V. Sarantsev. *Eur. Phys. J.*, A16:229, 2003.
[23] R. Kaminski, L. Lesniak, and B. Loiseau. *Eur. Phys. J.*, C9:141, 1999.
R. Kaminski, L. Lesniak, and J. P. Maillet. *Phys. Rev.*, D50:3145, 1994.